sciendo

On local aromaticity of selected model aza-[n]circulenes (n = 6, 7, 8 and 9): Density functional theoretical study

Denisa Cagardová, Vladimír Lukeš, Ján Matúška, Peter Poliak

Faculty of Chemical and Food Technology, Slovak University of Technology in Bratislava, Radlinského 9, SK-812 37 Bratislava, Slovakia
denisa.cagardova@stuba.sk

Abstract: A computational study using density functional theory is reported for selected model aza[n]circulenes (n = 6, 7, 8 and 9) and their derivatives consisting of pyrrole and benzene units. Local aromaticity of central rings was discussed and analyzed using theoretical structural indices. Depending on their molecular structures, energies of the highest occupied and lowest unoccupied molecular orbitals change from –5.23 eV to –4.08 eV and from –1.97 eV to –0.41 eV, respectively. Based on B3LYP calculated optimal geometries, electronic structure of molecules and their charge transport properties resulted in the suggestion of three planar molecules containing three or four pyrrole units as potential candidates for p-type semiconductors. Hole drift mobilities for ideal stacked dimers of these potential semiconductors were calculated and they range from 0.94 $cm^2 \cdot V^{-1} \cdot s^{-1}$ to 7.33 $cm^2 \cdot V^{-1} \cdot s^{-1}$.

Keywords: aromaticity index, HOMED, hole mobility, molecular orbitals, reorganization energy

Introduction

Hydrocarbon [n]circulenes represent a group of fully conjugated polycyclic compounds characterized by a central ring with [n] sides surrounded by ortho-fused benzene rings (Hensel et al., 2015). Nowadays, synthesized [n]circulenes and their π-extended derivatives include bowl-shaped [4]circulene (Bharat et al., 2010) and [5]circulene (Barth and Lawton, 1996), planar [6]circulene (Scholl and Meyer, 1932), saddle-shaped [7]circulene (Yamamoto et al., 1983) and [8]circulene (Feng et al., 2013). Optimal geometries of all hydrocarbon [n]circulenes from [3]circulene to [20]circulene were theoretically predicted by Christoph and co-workers (Christoph et al., 2008), who described the dependence of strain energy on the enlargement of the [n]circulene structure compared to the energy of [6]circulene using the Density Functional Theory (DFT) to predict molecular structure and implied properties. On the other hand, the existence of [3]circulene is considered to be unfeasible.

Replacing outer fused benzene rings by heterocyclic rings results in planar condensed heterocyclic compounds with highly π-conjugated electronic structures which can eventually be used in many important applications (Huong et al., 2015). Octathio[8]circulene ($C_{16}S_8$), called "sulflower", is a promising compound for optoelectronic applications, where all fused benzene rings are replaced by eight fused thiophene rings. It was synthesized in 2006 for the first time (Chernichenko et al., 2006). This compound was found to be a promising p-type organic semiconductor by both experimental and theoretical approaches (Dadvand et al., 2008; Datta and Pati, 2007). Subsequently, electronic structure and charge transport properties of various tetra-hetero[8]circulenes have also been extensively studied (Mohakud and Pati, 2009; Gahungu et al., 2009; Huong et al., 2012). Among them, organic molecules as azatrioxa-, diazadioxa-, diazadithia-, diazadiselena-[8]circulenes and tetrabenzotetraaza[8]circulene (Xiong et al., 2017; Sakamoto and Suzuki, 2013) have also attracted considerable attention because of functional motifs based on the unique optical and electronic properties of pyrroles. All the above mentioned heterocyclic [8]circulenes were suggested as either p-type or n-type organic semiconducting materials.

The concept of aromaticity is fundamental to rationalize and understand the electronic structure of compounds containing fused benzene and heterocyclic rings. It has been studied and characterized by many theoretical and organic chemists. Electronic structure of aromatic molecules can be investigated and described using different experimental techniques and theoretical methods. From the theoretical point of view, DFT represents one of many chemical approaches for the quantification of electron structure of conjugated systems with moderate computational cost (Hohenberg and Kohn, 1964; Runge and Gross, 1984). The DFT method is convenient for the gas-phase optimal geometry investigation of large molecules because

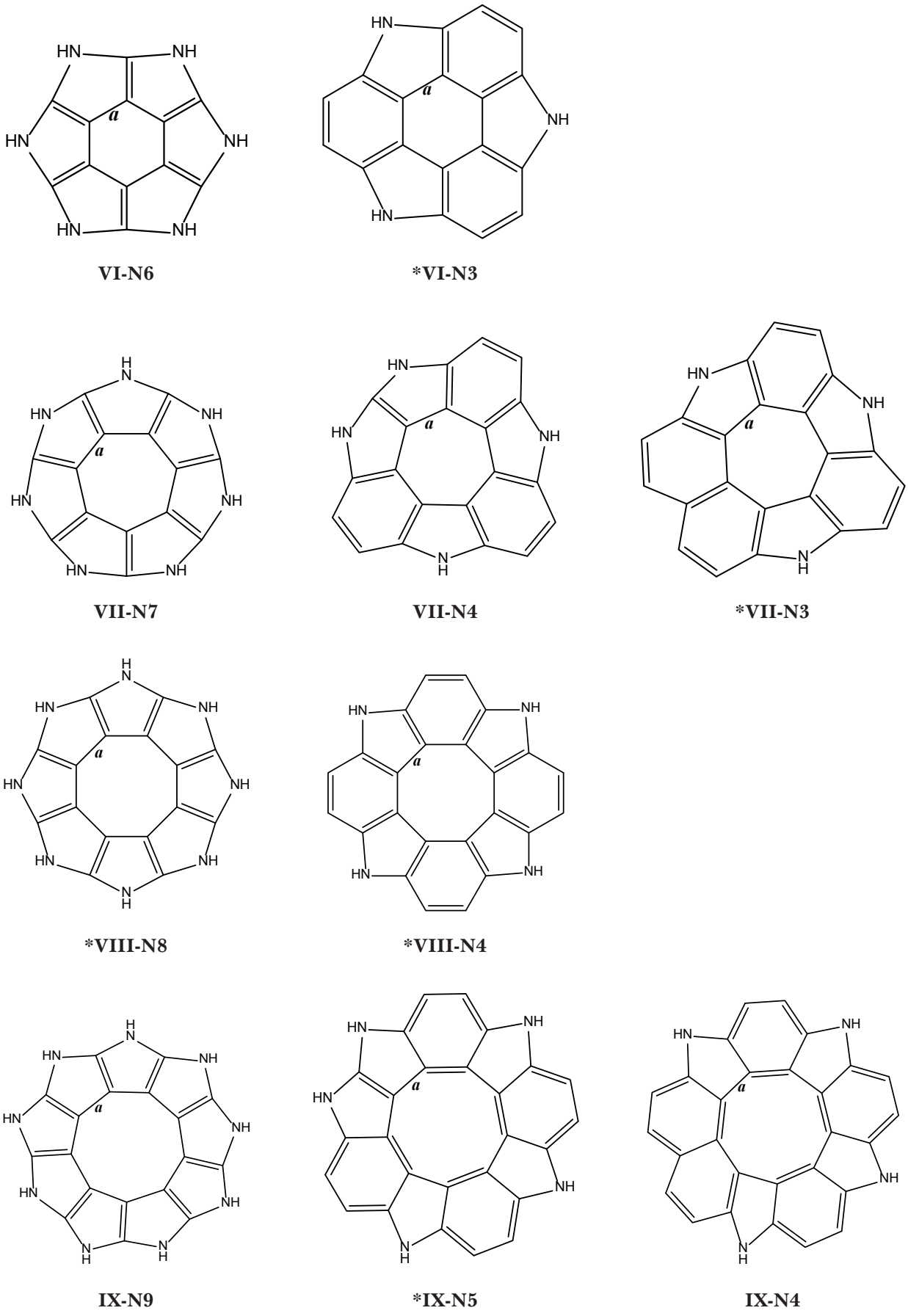

Fig. 1. Schematic structures of studied molecules and bond notation of central ring. Bonds (*a–i*) are ordered in clockwise direction. Asterisk symbol (*) indicates the planar B3LYP geometry.

it includes most effects of electron correlation. Although the electronic structure of various aza-[8] circulenes has been well characterized theoretically, systematic theoretical comparative study on model aza-[n]circulenes (n = 6, 7 and 9) and their derivatives is absent in literature.

With respect to this fact, we decided to present a theoretical analysis of electronic structures of the model series of ten aza-[n]circulenes (n = 6, 7, 8 and 9) and their derivatives (Fig. 1). Partial aims of this study are: (1) to calculate optimal geometries; 2) evaluate energies of frontier molecular orbitals and visualize their shapes and (3) calculate reorganization energies and drift mobilities. Consequently, the local aromaticity of central rings is discussed and hole mobilities are evaluated for selected model π-stacking configurations of dimers.

Quantum chemical calculations method

Quantum chemical calculations were performed using the Gaussian 09 program package (Frisch et al., 2010). Optimal geometries of the studied molecules were calculated by the DFT method with B3LYP (Becke's three parameter Lee—Yang—Parr) (Lee et al., 1988; Becke, 1988) functional without any constraints with the energy cut-off of 10^{-5} kJ · mol^{-1} and final RMS energy gradient below 0.01 kJ · mol^{-1} · A^{-1}. For open-shell systems, such as cations and anions, the unrestricted formalism (UB3LYP) was used. The SVP/SVPFit basis set of atomic orbitals was applied for all atoms (Eichkorn et al., 1995; Eichkorn et al., 1997). Next, the basis set for nitrogen atoms was minimally augmented with diffuse s- and p- functions by the set of diffusion functions in a systematic way (exponents of functions set to 1/3 of the exponent of the lowest function in the non-augmented basis set) (Zheng et al., 2011). Optimized structures were confirmed to be stable by vibrational analysis (no imaginary vibrations). For the model π-dimers, the interaction energy was corrected on Basis Set Superposition Error (BSSE) (Boys and Bernardi, 1970) using the Counterpoise method (Simon et al., 1996; Xantheas et al., 1996) and the B3LYP-D functional including the Grimme's dispersion D3 corrections on the van der Waals interactions was used (Grimme et al., 2010). The corresponding keyword in Gaussian input was GD3BJ. Molecules and molecular orbitals were visualized using the Molekel program package (Flukiger et al.; 2002).

Strain energies of the molecules were calculated to characterize structure modification of molecules in comparison with fixed planar structure, which is defined as the difference between electronic B3LYP energy of optimal geometry and electronic B3LYP energy of planar geometry with fixed atom arrangement.

One possible way of central ring aromaticity quantification is to express the geometrical changes of carbon-carbon bond lengths with respect to the structural changes using the Harmonic Oscillator Model of Electron Delocalization (HOMED) index (Frizzo and Martins, 2012)

$$\mathrm{HOMED} = 1 - \frac{\alpha}{j}\left\{\sum_{i=1}^{j}\left(R_{\mathrm{ref}} - R_{\mathrm{i}}\right)^2\right\} \tag{1}$$

where j represents the number of bonds considered and R_{i} is the actual carbon-carbon bond length (see Tab. 1). The B3YPL/SVP/SVPFit optimized reference carbon-carbon bond length (R_{ref}) obtained from the benzene molecule is of 1.3988 Å. The normalization constant, α, was calculated using the following equation (Ośmiałowski et al., 2006)

$$\alpha = 2\left\{\left(R_{\mathrm{ref}} - R_{\mathrm{sin}}\right)^2 + \left(R_{\mathrm{ref}} - R_{\mathrm{doub}}\right)^2\right\}^{-1} \tag{2}$$

where the reference single bond R_{sin} and the reference double bond R_{doub} were estimated from ethane and ethene molecules respectively. Our calculated single C—C and double C═C bond lengths were 1.5277 Å and 1.3330 Å, respectively. Based on these bond lengths, the normalization constant is of 95.6 Å^{-2}.

Internal reorganization energy ($\lambda^{\pm}$) is another important quantity describing structural changes in molecules upon electron abstraction or addition. These energies refer to the energy required for geometry relaxation from the electroneutral to charged state of molecule and *vice versa* (Brédas et al., 2004; Wang et al., 2014; Da Silva Filho et al., 2005; Marcus, 1993). Based on the optimized electroneutral molecule and cation/anion geometries, reorganization energies are given by the equation

$$\begin{aligned}\lambda^{\pm} &= \lambda_1^{\pm} + \lambda_2^{\pm} = \\ &= \left[E_{\pm}(Q_N) - E_{\pm}(Q_{\pm})\right] + \left[E_N(Q_{\pm}) - E_N(Q_N)\right]\end{aligned} \tag{3}$$

where $E_{\pm}(Q_N)$ is the total energy of charged state in the electroneutral geometry, $E_{\pm}(Q_{\pm})$ is the total energy of the charged state in the charged state geometry, $E_N(Q_{\pm})$ is the total energy of the neutral state in the charged state geometry, and $E_N(Q_N)$ is the total energy of the electroneutral state in the neutral geometry (Malagoli et al., 2004; Brédas et al., 2004).

To describe conductive properties, the hole-transfer rate, k_{hole}, between two interacting subsystems can be evaluated using classical Marcus formula (Marcus, 1993; Sakanoue et al., 1999; Malagoli and Brédas, 2000)

Tab. 1. Selected B3LYP/SVP/SVPFit optimal bond lengths (in Ångstroms) and HOMED parameters of central rings of all studied molecules.

Molecule	*a*	*b*	*c*	*d*	*e*	*f*	*g*	*h*	*i*	HOMED
VI-N3	1.3773	1.3572	1.3773	1.3573	1.3772	1.3572				0.8950
VII-N3	1.4057	1.3839	1.4259	1.4204	1.4205	1.4258	1.3839			0.9606
VII-N4	1.3940	1.4332	1.4055	1.4332	1.3940	1.4130	1.4130			0.9610
VIII-N4	1.4151	1.4409	1.4151	1.4410	1.4151	1.4409	1.4151	1.4410		0.9026
IX-N4	1.4677	1.4877	1.4444	1.4597	1.4311	1.4597	1.4444	1.4877	1.4676	0.5979
IX-N5	1.4680	1.4533	1.4870	1.4533	1.4680	1.4249	1.4453	1.4453	1.4249	0.6926
VI-N6	1.4641	1.4389	1.4389	1.4641	1.4389	1.4389				0.7621
VII-N7	1.4378	1.4378	1.4303	1.4483	1.4283	1.4484	1.4301			0.8529
VIII-N8	1.3624	1.3625	1.3624	1.3625	1.3624	1.3625	1.3624	1.3625		0.8734
IX-N9	1.4300	1.4274	1.4278	1.4296	1.4259	1.4320	1.4249	1.4323	1.4257	0.9159

$$k_{hole} = t^2 \left(\frac{\pi}{\hbar^2 k_B \lambda^+ T} \right)^{1/2} \exp\left(-\frac{\lambda^+}{4 k_B T} \right) \quad (4)$$

where t represents an intermolecular hole-transfer integral between the interacting molecular sites, $\hbar$ is the reduced Planck constant, k_B is the Boltzmann constant, T is the thermodynamic temperature and λ^+ represents the hole reorganization energy. The hole-transfer integrals for optimal dimer geometries were calculated in the one-electron approximation using the direct evaluation method (Nan et al., 2011).

At constant temperature, the hole drift mobility, μ_{hole}, can be calculated by the Einstein—Smoluchowski relation (Maier and Ankerhold, 2010; Cornil et al., 2002)

$$\mu_{hole} = \frac{e}{k_B T} \frac{1}{2m} k_{hole} d^2 \quad (5)$$

where e is the elementary charge. The length of hopping pathway, d, is defined as the centroid-to-centroid distance. Symbol m stands for space dimensionality and k_{hole} is the hole-transfer rate. Considering a two-dimensional transfer, m value equals 2.

Results and Discussion

Chemical structure

Chemical structure of the investigated molecules depends on the size of their central ring as well as on the number of outer heterocyclic units. According to the notation in Fig. 1, symmetric [n]aza-[n]heterocirculenes containing [n] pyrrole units (n = 6, 7 and 9) are distorted and exhibit bowl-shaped structures (**VI-N6, VII-N7** and **IX-N9**, respectively). Within the group of studied [n]aza-[n]heterocirculenes, the **VIII-N8** molecule is planar. Only the **IX-N4** molecule shows a saddle-shaped optimal geometry. Interestingly, theoretical results obtained for fully [n]thiophenyl-[n]circulenes showed planarity and minimal strain energy for molecules containing eight and nine thiophene rings (Chernichenko et al., 2006). In case of the remaining investigated molecules, separation of pyrrole units by benzene ring supports the planarity for almost all [n/2]aza[n]circulenes (n = 6, 8). The theoretically predicted planar structure of the **VIII-N4** molecule is in agreement with the X-ray structure of alkyl substituted tetraaza-[8]circulene (Nagata et al., 2017). The largest **IX-N5** molecule is planar because of two condensed pyrrole rings which results in the strain decrease in the central ring compared with **IX-N4**. Interestingly, planarity of **VII-N3** is caused by two condensed benzene rings in its structure. Generally, planarity of a molecule is supported by lower strain in the structure characterized by strain energies and dihedral angles. Strain energies, ΔE_s, calculated with respect to the fixed planar geometries changed from 57.3 kJ·mol^{-1} to 210 kJ·mol^{-1} for the bowl-type structures (Fig. 2). Only one molecule, **IX-N4,** exhibited the saddle-type structure and the corresponding strain energy was 17.6 kJ·mol^{-1}. Dihedral angles studied are defined by three atoms from the central ring characterizing one plane, the fourth atom is carbon in fused pyrrole rings (see Fig. 2). Bowl-shaped molecule **VI-N6** provides the smallest range of dihedral angles (118—126 °) and so it is obvious that this molecule has the most significant strain (with strain energy of 210 kJ·mol^{-1}) compared with its fixed planar structure. On the other hand, in case of the **IX-N9** molecule, dihedral angles are in the range from 143 ° to 153 ° and its strain energy is of 57.3 kJ·mol^{-1}, which means that this molecule is not significantly deformed related to the planar structure.

Although the pyrrole and benzene building units have aromatic character, central rings of the studied aza-[n]circulenes do not have to be aromatic. The

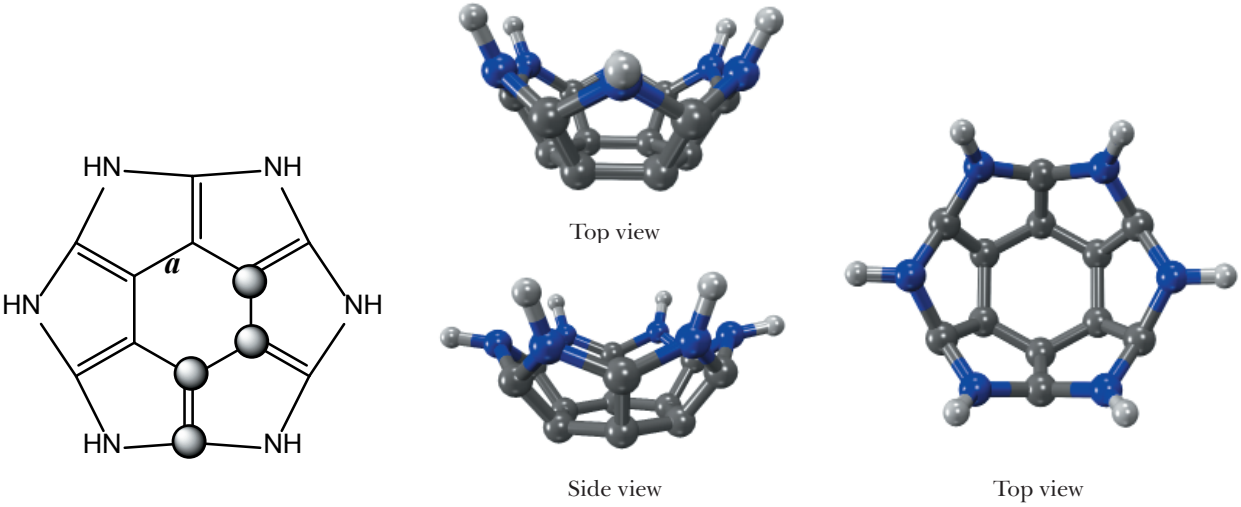

VI-N6 (ΔE_s = 210.0 kJ · mol^{-1}; ϑ = 118–126 °)

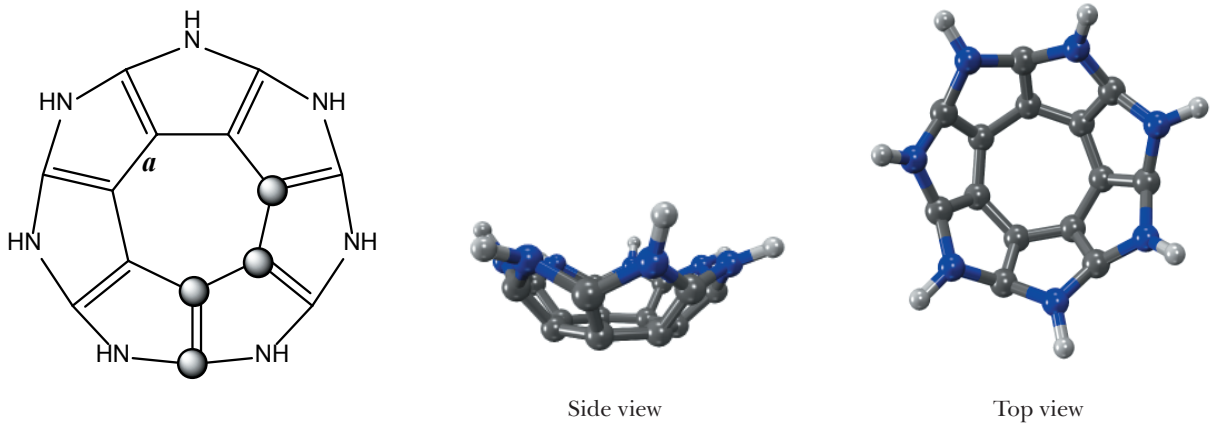

VII-N7 (ΔE_s = 165.4 kJ · mol^{-1}; ϑ = 127–135 °)

VII-N4 (ΔE_s = 196.5 kJ · mol^{-1}; ϑ = 142–161 °)

Fig. 2. Front and side views of the investigated non-planar molecules. B3LYP strain energies ΔE_s and dihedral angles ϑ are written in parentheses. Grey balls (on left) symbolize carbon atoms providing a dihedral angle ϑ. Corresponding colors of atoms: black – carbon, white – hydrogen, blue – nitrogen.

HOMED parameters evaluated for the central molecular rings of the studied molecules exhibit differences in the π-electron delocalization. An increase of the HOMED index is related to significant increase of π-electron delocalization in molecular structures. Comparison of the HOMED parameters collected in Tab. 1 shows that **VII-N3** and **VII-N4** molecules exhibit the highest HOMED values of 0.96. On the other hand, the less aromatic character (HOMED = 0.60) results in the saddle-shaped **IX-N4** molecule. Interestingly, molecular planarity does not depend on the aromaticity of the central ring.

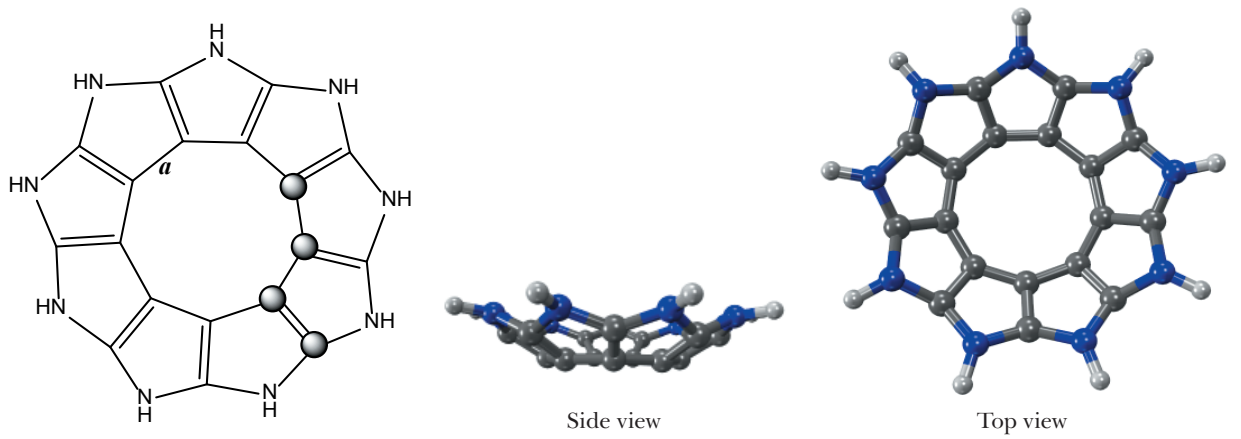

IX-N9 (ΔE_s = 57.3 kJ · mol^{-1}; ϑ = 143—153 °)

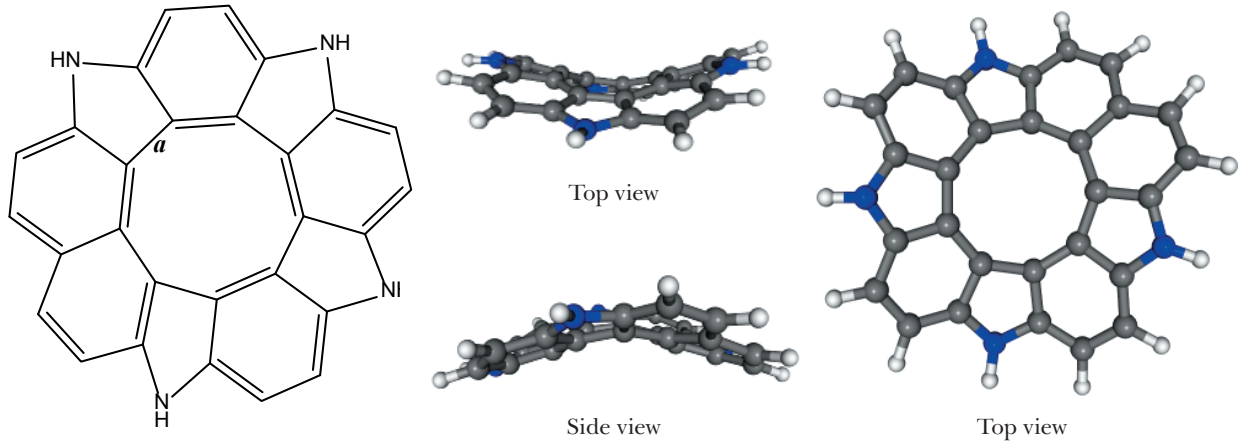

IX-N4 (ΔE_s = 17.6 kJ · mol^{-1})

Fig. 2. (continued) Front and side views of the investigated non-planar molecules. B3LYP strain energies ΔE_s and dihedral angles ϑ are written in parentheses. Grey balls (on left) symbolize carbon atoms providing dihedral angle ϑ. Corresponding colors of atoms: black — carbon, white — hydrogen, blue — nitrogen.

Calculated values of energy parameters for both charged states are listed in Tab. 2. For planar molecules, the B3LYP hole reorganization energy, λ^+, connected with the formation of cationic state varies from 0.144 eV for **IX-N5** to 0.332 eV for **VII-N3**. In case of bowl-shaped molecules, the **VII-N7** molecule has the highest value of λ^+ (0.713 eV). The saddle shaped molecule **IX-N9** provides the hole reorganization energy of 0.638 eV. In case of anionic state formation, the electron reorganization energies, λ^-, change from 0.167 eV for the planar **VIII-N8** molecule to 0.685 eV for the bowl-shaped **VI-N6** molecule. The hole reorganization energy decreases as the size of the π-conjugated system increases. The presented results are in good agreement with the general trends suggested in literature. For example, the calculated intramolecular hole reorganization energy for an isolated tetracene is of 0.114 eV (Da Silva Filho et al., 2005), which is nearly by 30 % lower than that of the rubrene molecule (0.159 eV) containing four perpendicularly oriented phenyl rings. However, these values remain significantly lower than that of bis-(triarylamine) derivative of tetraphenyl-diamino-biphenyl (TPD) (0.290 eV) (Malagoli et al., 2004), a well-established hole-transport material. The low electron reorganization energy of fullerenes can also be attributed to their extended π-conjugation and their rigid molecular structures. For example, the C_{60} molecule has been found to be an excellent n-type acceptor with low electron reorganization energy of 0.060 eV (Larsson et al., 1998). On the other hand, theoretical B3LYP λ^- values reported for donor-acceptor 1,8-naphthalimide derivatives are of 0.216—0.235 eV (Chai and Jin, 2016). For a smaller fluorinated pentacene, the electron reorganization energy is of 0.246 eV (Lukeš et al., 2018) and for tris(8-hydroxyquinolinato)aluminum (Alq_3) it is of 0.296 eV (Friederich et al., 2016).

Table 2: Vertical ionization potentials (*VIP*), adiabatic ionization potentials (*AIP*), vertical electron affinities (*VEA*), adiabatic electron affinities (*AEA*), reorganization energies for hole and electron transfer (λ^+ and λ^-, respectively) of studied molecules. All energies are in eV. Asterisks (*) indicate planar molecules.

Molecule	*VIP*	*AIP*	*VEA*	*AEA*	λ^+	λ^-
***VI-N3**	6.727	6.640	–0.593	–0.471	0.181	0.245
***VII-N3**	6.400	6.150	–0.156	–0.055	0.332	0.205
VII-N4	6.279	6.014	–0.278	–0.114	0.421	0.339
***VIII-N4**	6.309	6.233	0.237	0.329	0.149	0.184
IX-N4	5.923	5.830	0.058	0.185	0.176	0.262
***IX-N5**	5.614	5.542	–0.291	–0.200	0.144	0.183
VI-N6	6.259	5.958	0.368	0.793	0.598	0.685
VII-N7	6.233	5.880	–0.040	0.268	0.713	0.606
***VIII-N8**	5.646	5.537	–0.250	–0.169	0.220	0.167
IX-N9	5.480	5.136	–0.829	–0.620	0.638	0.645

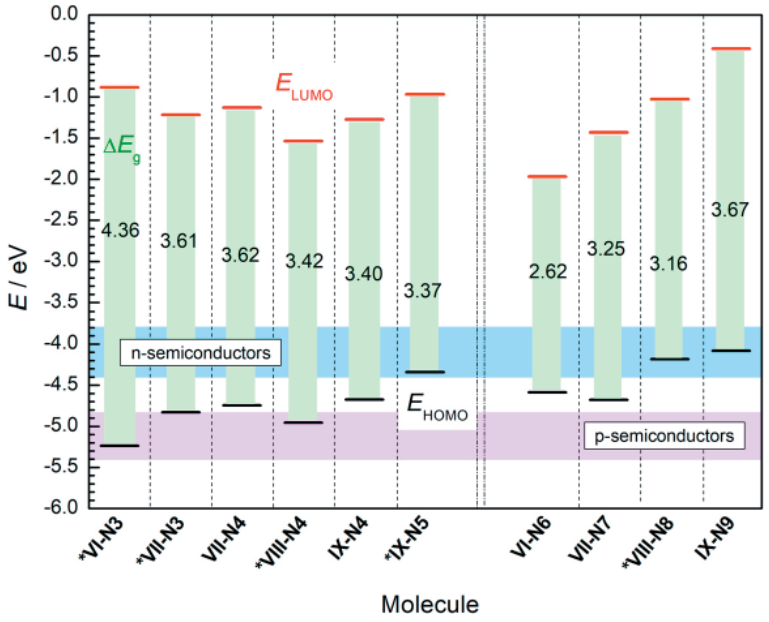

Fig. 3. Energy diagram of B3LYP/SVP frontier molecular orbitals for electroneutral states of studied molecules. HOMO—LUMO energy gaps ΔE_g (green band) are in eV. Asterisks (*) indicate planar molecules.

Frontier molecular orbitals

Energy levels of frontier molecular orbitals have direct influence on the carrier injection ability and oxidation stability of the material. Based on the B3LYP/SVP optimized structures of the electroneutral state, energy levels of the Highest Occupied (HOMO) and Lowest Unoccupied (LUMO) Molecular Orbitals were calculated. The obtained results and corresponding energy gaps (ΔE_g) for all molecules are depicted in Fig. 3. Enlargement of molecular structures with respect to the number of building aromatic units significantly affects the energy of frontier molecular orbitals. However, there is no significant trend. In Fig. 3, the depicted blue bars represent LUMO energies within the energy interval from –4.4 eV to –3.8 eV, which are suitable to stabilize electrons during charge transfer in electron transport materials (Liu et al., 2010; Chang et al., 2010; Murphy and Fréchet, 2007). Our theoretical calculations showed that LUMO energies vary between –2.0 eV and –0.4 eV. These values do not meet the above-mentioned criteria; thus it is not an optimal setting for n-type semiconductivity.

On the other hand, the depicted pink bars indicate the range of HOMO energy values typical for commercial p-type organic semiconductors. For example, the reported HOMO energies of

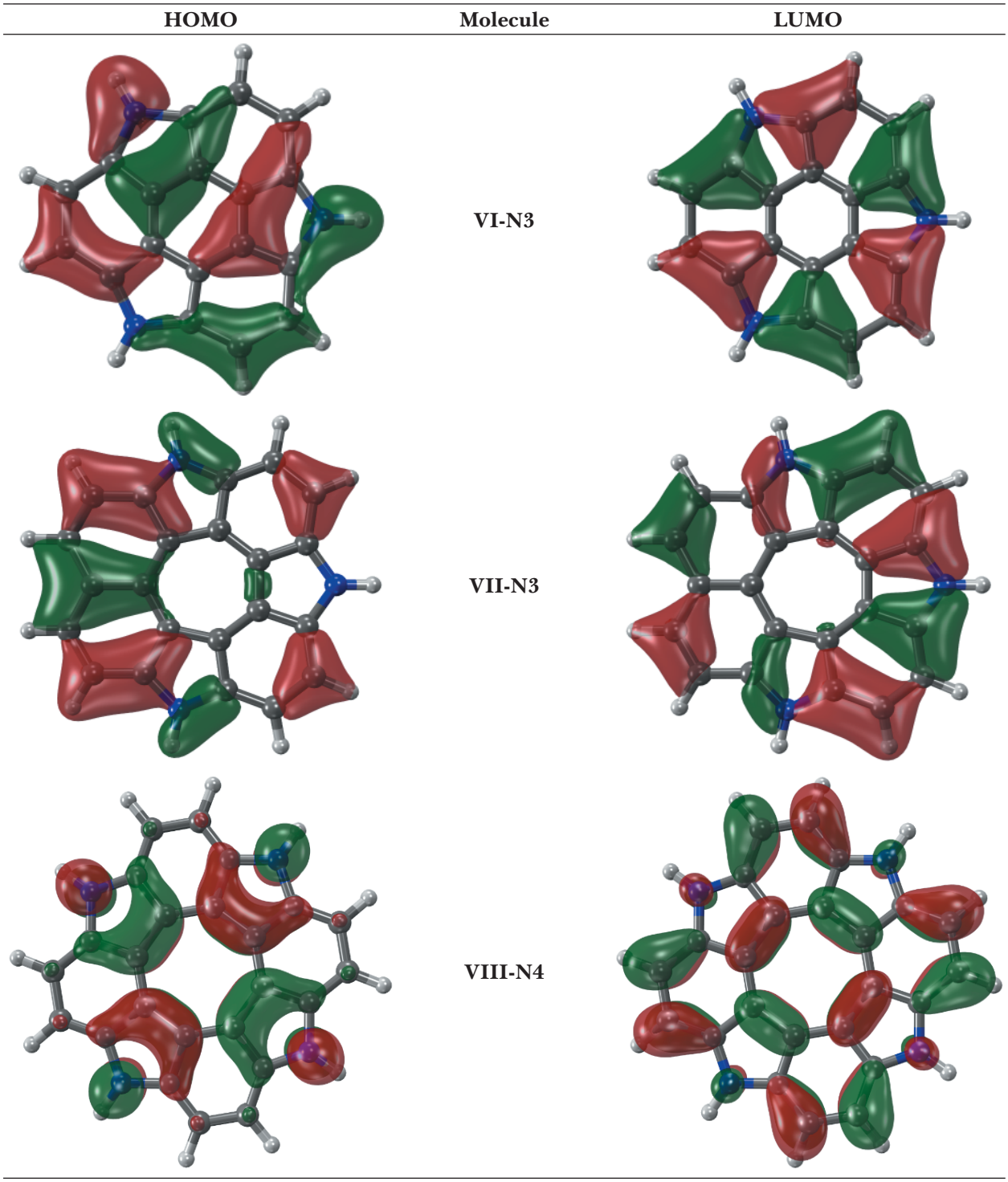

Fig. 4. Shapes of B3LYP frontier molecular orbitals for selected electroneutral planar molecules **VI-N3**, **VII-N3** and **VIII-N4**. Corresponding colors of atoms: black — carbon, white — hydrogen, blue — nitrogen. Depicted iso-surface value is 0.025 a.u.

α-sexithiophene and pentacene are of –5.3 eV and –5.0 eV (Sigma Aldrich, 2019), respectively. In case of the smallest planar **VI-N3** molecule, the B3LYP HOMO energy is of –5.26 eV and it is the lowest HOMO energy compared with the remaining studied molecules. The corresponding LUMO energy is of –0.90 eV. The maximal value of HOMO is of –4.10 eV for the saddle-shaped **IX-N9** molecule. Based on our results, HOMO energies of **VII-N3**, **VIII-N4** and **VI-N3** fall within the interval of HOMO energies typical for p-semiconductors (see Fig. 3).

The HOMO–LUMO energy gap (ΔE_g) value represents a theoretical parameter which corresponds to the electrochemical gap. The B3LYP/SVP ΔE_g energy is the highest for the smallest planar molecule **VI-N3** (4.36 eV) and the lowest for the bowl-shaped **VI-N6** molecule (2.62 eV).

With respect to the above-mentioned criteria, molecules **VII-N3**, **VIII-N4** and **VI-N3** could be used as potential p-type semiconductors because of their low reorganization energies and their HOMO energies falling within the interval typical for p-semiconductor LUMO energies. Moreover, planarity of these molecules supports their potential application in optoelectronics.

Shapes of frontier molecular orbitals of selected planar **VII-N3**, **VIII-N4** and **VI-N3** molecules reveal the typical π-type molecular orbital character. As it is demonstrated in Fig. 4 for the above-mentioned promising molecules, the lobes of HOMO for larger **VII-N3** and **VIII-N4** molecules

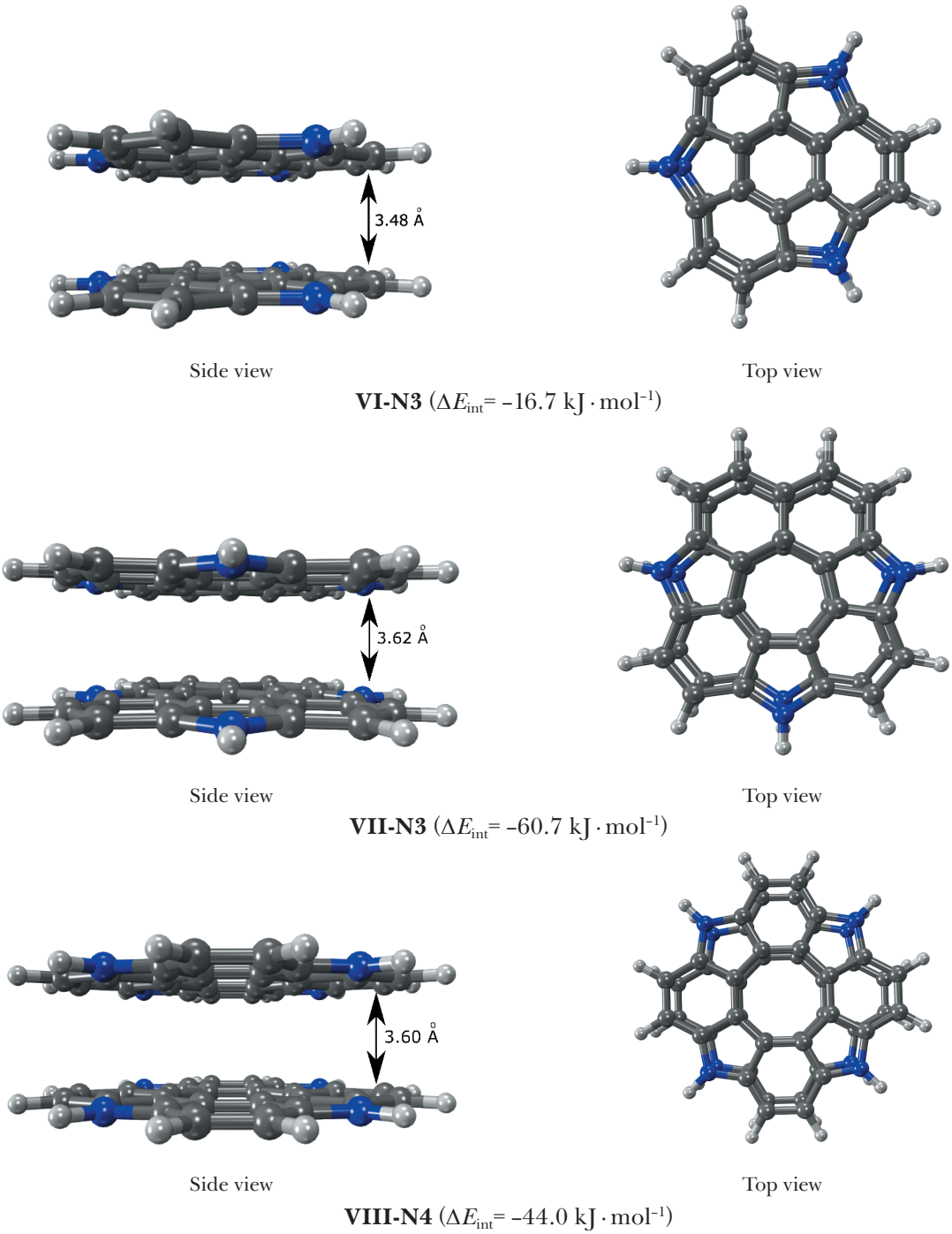

Fig. 5. Side and top views of optimal geometries of model sandwich dimer configurations of **VI-N3**, **VII-N3** and **VIII-N4**. Counterpoise corrected B3LYP-D interaction energies ΔE_{int} are written in parentheses. Corresponding colors of atoms: black — carbon, white — hydrogen, blue — nitrogen.

are spoke-wheel oriented towards the central ring. Probably, the different shape of electron delocalization in the smallest **VI-N3** molecule is related to lower aromaticity of its central ring (see Tab. 1). A similar situation occurs in the delocalization of LUMO clouds where electrons are depleted from nitrogen atoms of pyrrole units. Interestingly, an increase of central ring HOMED causes a decrease of energy gaps of molecules.

Electrochemical properties of the investigated organic molecules as well as their air stability are also proportionally related to their ionization potentials (*IPs*) and electron affinities (*EAs*). These quantities are commonly used for the interpretation of electric solid-state experiments. According to previous studies, the adiabatic *IP* (*AIP*) of the selected air-stable p-type materials ranges from 5.9 eV to 6.8 eV, while the adiabatic *EA* (*AEA*) for the air-stable n-type ones should be lower than 4.0 eV but higher than 2.8 eV (Liu et al., 2010; Chang et al., 2010). The comparison of vertical ionization potentials (*VIP*), vertical electron affinities (*VEA*), adiabatic ionization potentials (*AIP*) and adiabatic electron affinities (*AEA*) listed in Tab. 2 supports the findings obtained from the analysis of energies of frontier molecular orbitals. The studied molecules are unsuitable organic n-semiconductors. However, the planar **VII-N3**, **VIII-N4** and **VI-N3** molecules could be perspective as p-type semiconductors.

Electric mobilities

Macroscopic properties of solid materials strongly depend on the internal molecular structure. However, it is impossible to calculate the exact value of microscopic electric quantities because they represent the statistical average value of local molecular assemblies. To estimate and compare the p-type semiconducting properties of selected perspective molecules (**VII-N3**, **VIII-N4** and **VI-N3**), model dimers in perfectly parallel-stacked configuration were investigated. As it is indicated in Fig. 5, the optimal intermolecular distances between molecular planes are of 3.48 Å, 3.60 Å and 3.62 Å for **VI-N3**, **VIII-N4** and **VII-N3** sandwich dimers, respectively. The corresponding interaction energies are of –16.7 kJ · mol^{-1} for **VI-N3**, –60.7 kJ · mol^{-1} for **VII-N3** and –44.0 kJ · mol^{-1} for **VIII-N4**.

Hole-transfer integrals reach values of 0.302 eV for **VI-N3**, 0.253 eV for **VII-N3** and 0.216 eV for **VIII-N4**. Consequently, according to equation (4), the hole-transfer rates are of 6.15 × 10^{14} s^{-1} for **VI-N3**, 0.74 × 10^{14} s^{-1} for **VII-N3** and 4.78 × 10^{14} s^{-1} for **VIII-N4**.

The drift hole mobilities evaluated by equation (5) for optimal geometries at T = 298 K are 7.33 cm^2 · V^{-1} · s^{-1} for **VI-N3**, 0.94 cm^2 · V^{-1} · s^{-1} for **VII-N3** and 6.02 cm^2 · V^{-1} · s^{-1} for **VIII-N4**. Additionally, the hole drift mobilities dependence on the distance between planes in the vicinity of the minimal interaction energy of an ideal dimer, i.e. d between 3 to 4 Å, was studied because the displacement between the molecular units can vary in real solid materials. As it is illustrated in Fig. 6, exponential decrease of the hole drift mobilities occurred given by:

$$\mu_{hole} = A\exp(-Bd) \tag{6}$$

Correlation coefficients of the fitted function are above 0.999. The lowest value of the preexpo-

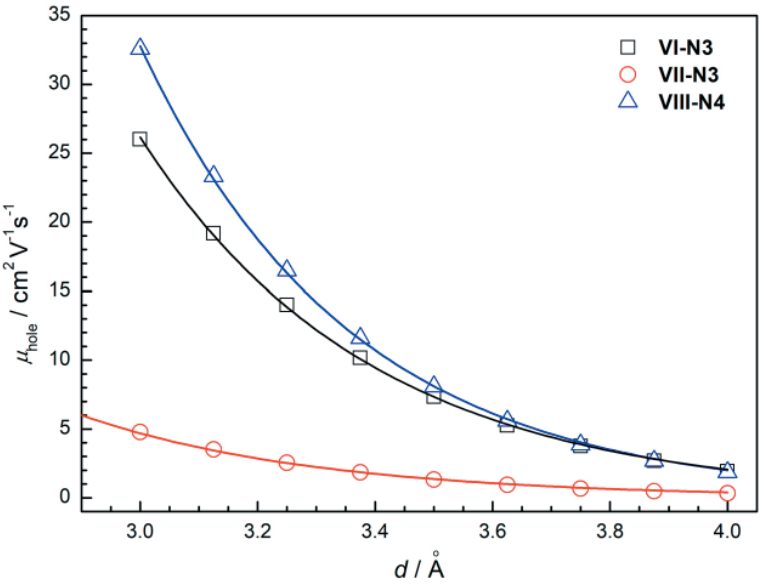

Fig. 6. Dependence of hole electric mobilities on the distance for promising model dimers of **VI-N3**, **VII-N3** and **VIII-N4**.

nential factor *A* was found for the **VII-N3** dimer and its value is of $(7.7 \pm 0.6) \times 10^3\ cm^2 \cdot V^{-1} \cdot s^{-1}$. These values for **VI-N3** and **VIII-N4** dimers are of $(54 \pm 4) \times 10^3\ cm^2 \cdot V^{-1} \cdot s^{-1}$ and $(14 \pm 1) \times 10^4\ cm^2 \cdot V^{-1} \cdot s^{-1}$, respectively. Exponent arguments *B* (in $Å^{-1}$) are of 2.47 ± 0.03 for the **VII-N3** dimer, 2.54 ± 0.02 for the **VI-N3** dimer and 2.79 ± 0.03 for the **VIII-N4** sandwich dimer. It seems that the magnitude order of obtained values is comparable with the theoretical and experimental values reported in literature for hole mobility of typical organic p-type semiconductors. For example, the hole drift mobility simulated for perfect coronene and pentacene stacks were found to be 14.93 $cm^2 \cdot V^{-1} \cdot s^{-1}$ (Bag and Maiti, 2017) and 12.54 $cm^2 \cdot V^{-1} \cdot s^{-1}$ (Lukeš et al., 2018), respectively. However, experimental results for pentacene film layers are between 0.3 and 3.0 $cm^2 \cdot V^{-1} \cdot s^{-1}$ depending on the temperature and construction of field-effect transistors (Lin et al., 1997; Yakuphanoglu et al., 2012).

Conclusions

Ten model aza-[n]circulenes (n = 6, 7, 8 and 9) and their derivatives were studied at the density functional theory level. The obtained theoretical data show that local aromaticity of the central ring is strongly dependent on the number of benzene and pyrrole units and on their mutual position. The minimal steric repulsion among the aryl rings were found for the **VI-N3**, **VII-N3**, **VIII-N4**, **VIII-N8** and **IX-N5** molecules. Depending on the molecular structure, energies of the highest occupied and lowest unoccupied molecular orbitals change from –5.23 eV to –4.08 eV and from –1.97 eV to –0.41 eV, respectively. A comparison of frontier molecular orbital energies, ionization potentials and electron affinities with data for typical organic semiconductors showed that none of the studied molecules are suitable to be n-type semiconductors. On the other hand, based on the calculated electric properties, planar **VII-N3**, **VIII-N4** and **VI-N3** molecules are potential p-type semiconductors. For perfect-stacked sandwich dimers at optimal centroid-to-centroid distance, the hole drift mobility evaluated is maximal for **VI-N3** with the value of 7.33 $cm^2 \cdot V^{-1} \cdot s^{-1}$. Molecule **VII-N3** provides significantly lower hole drift mobility of 0.94 $cm^2 \cdot V^{-1} \cdot s^{-1}$.

Acknowledgment

The work has been supported by the Slovak Research and Development Agency (APVV-15-0053). The authors would like to thank for financial contribution from the STU Grant scheme for the Support of Young Researchers (1619). We are grateful to the HPC center at the Slovak University of Technology in Bratislava, which is a part of the Slovak Infrastructure of High Performance Computing (SIVVP project, ITMS code 26230120002, funded by the European region development funds, ERDF) for the computational time and resources made available.

References

Bag S, Maiti PK (2017) Phys. Rev. B 96(24): 245401. Doi: https://doi.org/10.1103/PhysRevB.96.245401.

Barth WE, Lawton RG (1966) J. Am. Chem. Soc. 88:380. Doi: https://doi.org/10.1021/ja00954a049.

Becke AD (1988) Phys Rev A 38: 3098—3100. Doi: https://doi.org/10.1103/PhysRevA.38.3098.

Bharat, Bhola, R, Bally T, Valente A, Cyrański MK, Dobrzycki Ł, Spain SM, Rempała P, Chin MR, King BT (2010) Angew. Chem. Int. Ed. 49: 399. Doi: https://doi.org/10.1002/anie.200905633.

Boys SF, Bernardi F (1970) Mol Phys 19: 553—566. Doi: https://doi.org/10.1080/00268977000101561.

Brédas JL, Beljonne D, Coropceanu V, Cornil J (2004) Chem Rev 104: 4971—5003. Doi: https://doi.org/10.1021/cr040084k.

Chai W, Jin R (2016) J. Mol. Struct. 1103: 177—182. Doi: https://doi.org/10.1016/j.molstruc.2015.09.023.

Chang YC, Kuo MY, Chen CP, Lu HF, Chao I (2010) J. Phys. Chem. C. 114: 11595—11601. Doi: https://doi.org/10.1021/jp1025625.

Chernichenko KY, Sumerin VV, Shpanchenko RV, Balenkova ES and Nenajdenko G (2006) Angew. Chem. 45(44): 7367—7370. Doi: https://doi.org/10.1002/anie.200602190.

Christoph H, Grunenberg J, Hopf H, Dix I, Jones PG, Scholtissek M, Maier G (2008) Chem. Eur. J. 14: 5604. Doi: https://doi.org/10.1002/chem.200701837.

Cornil J, Lemaur V, Calbert JP, Brédas JL (2002) Adv Mater 14: 726. Doi: https://doi.org/10.1002/1521-4095(200107)13:14<1053::AID-ADMA1053>3.0.CO;2-7.

Da Silva Filho DA, Kim EG, Brédas JL (2005) Adv. Mater. 17: 1072—1076. Doi: https://doi.org/10.1002/adma.200401866.

Dadvand A, Cicoira F, Chernichenko YK, Balenkova ES, Osuna RM, Rosei F, Nenajdenko VG, Perepichka DF (2008) Chem. Commun. 42: 5354—5356. Doi: https://doi.org/10.1039/B809259A.

Datta A, Pati SK (2007) J. Phys. Chem. C 19: 4487—4490. Doi: https://doi.org/10.1021/jp070609n.

Eichkorn K, Treutler O, Ohm H, Haser M, Ahlrichs R (1995) Chem. Phys. Lett., 240: 283—289. Doi: https://doi.org/10.1016/0009-2614(95)00621-A.

Eichkorn K, Weigend F, Treutler O, Ahlrichs R (1997) Theor. Chem. Acc. 97: 119—124. Doi: https://doi.org/10.1007/s002140050244.

Feng CN, Kuo MY, Wu YT (2013) Angew. Chem. Int. Ed. 52: 7791. Doi: https://doi.org/10.1002/anie.201303875.

Flukiger P, Luthi HP, Sortmann S, Weber J (2002) Molekel 4.3, Swiss National Supercomputing Centre, Manno, Switzerland.

Friederich P, Meded V, Poschlad A, Neumann T, Rodin V, Stehr V, Symalla F, Danilov D, Lüdemann G, Fink RF, Kondov I, von Wrochem F, Wenzel W (2016)

Adv. Funct. Mater. 26: 5757—5763. Doi: https://doi.org/10.1002/adfm.201601807.
Frisch MJ, Trucks GW, Schlegel HB, Scuseria GE, Robb MA, Cheeseman JR, Scalmani G, Barone V, Mennucci B, Petersson GA, Nakatsuji H, Caricato M, Li X, Hratchian HP, Izmaylov AF, Bloino J, Zheng G, Sonnenberg JL, Hada M, Ehara M, Toyota K, Fukuda R, Hasegawa J, Ishida M, Nakajima T, Honda Y, Kitao O, Nakai H, Vreven T, Montgomery JA Jr., Peralta JE, Ogliaro F, Bearpark M, Heyd JJ, Brothers E, Kudin KN, Staroverov VN, Keith T, Kobayashi R, Normand J, Raghavachari K, Rendell A, Burant JC, Iyengar SS, Tomasi J, Cossi M, Rega N, Millam JM, Klene M, Knox JE, Cross JB, Bakken V, Adamo C, Jaramillo J, Gomperts R, Stratmann RE, Yazyev O, Austin AJ, Cammi R, Pomelli C, Ochterski JW, Martin RL, Morokuma K, Zakrzewski VG, Voth GA, Salvador P, Dannenberg JJ, Dapprich S, Daniels AD, Farkas O, Foresman JB, Ortiz JV, Cioslowski J, Fox DJ (2009) Gaussian 09, Revision D.01, Gaussian Inc. Wallingford CT, Gaussian 09 Revis. C.01. (2010) Gaussian Inc., Wallingford CT. Doi: https://doi.org/10.1017/CBO9781107415324.004.
Frizzo CP, Martins MAP (2012) Struct Chem 23: 375—380. Doi: https://doi.org/10.1007/s11224-011-9883-z.
Gahungu G, Zhang J, Barancira T (2009) J. Phys. Chem. A 113: 255—262. Doi: https://doi.org/10.1021/jp804986b.
Grimme S, Antony J, Ehrlich S, Krieg H (2010) J Chem Phys 132(15): 154104. Doi: https://doi.org/10.1063/1.3382344.
Hensel T, Andersen NN, Plesner M, Pittelkow M (2016) Synlett. 27(04): 498—525. Doi: https://doi.org/10.1055/s-0035-1560524.
Hohenberg P, Kohn W (1964) Phys. Rev. 136: B864—B871. Doi: https://doi.org/10.1103/PhysRev.136.B864.
Huong VTT, Tai TB, Nguyen MT (2012) Phys. Chem. Chem. Phys. 14: 14832—14841. Doi: https://doi.org/10.1039/C2CP42474F.
Huong VTT, Tai TB, Nguyen MT (2015) RSC Adv. 5: 24167—24174. Doi: https://doi.org/10.1039/C4RA16485G.
Larsson S, Klimkans A, Rodriguez-Monge L, Duskesas G (1998) Theochem-Journal Mol. Struct. 425: 155—159. Doi: https://doi.org/10.1016/S0166-1280(97)00216-9.
Lee C, Yang W, Parr RG (1988) Phys Rev B 37: 785—789. Doi: https://doi.org/10.1103/PhysRevB.37.785.
Lin YY, Gundlach DJ, Nelson SF, Jackson TN (1997) IEEE Electron Device Lett. 18: 606—608. Doi: https://doi.org/10.1109/55.644085.
Liu CC, Mao SW, Kuo MY (2010) J. Phys. Chem. C. 114: 22316—22321. Doi: https://doi.org/10.1021/jp1099464.
Lukeš V, Cagardová D, Michalík M, Poliak P (2018) Synt. Met. 240: 67—76. Doi: https://doi.org/10.1016/j.synthmet.2018.03.014.
Maier SA, Ankerhold J (2010) Phys. Rev. E 81: 021107. doi: https://doi.org/10.1103/PhysRevE.81.021107.
Malagoli M, Brédas JL (2000) Chem Phys Lett 327: 13—17. Doi: https://doi.org/10.1016/S0009-2614(00)00757-0.
Malagoli M, Coropceanu V, Da Silva Filho DA, Brédas JL (2004) J. Chem. Phys. 120: 7490—7496. Doi: https://doi.org/10.1063/1.1687675.
Marcus RA (1993) Rev Mod Phys 65: 599—610. Doi: https://doi.org/10.1103/RevModPhys.65.599.
Mohakud S, Pati SK (2009) J. Mater. Chem.19: 4356—4361. Doi: https://doi.org/10.1039/B901014A.
Murphy AR, Fréchet JMJ (2007) Chem. Rev. 107: 1066—1096. Doi: https://doi.org/10.1021/cr0501386.
Nagata Y, Kato S, Miyake Y, Shinokubo H (2017) Org. Lett. 19: 2718—2721. Doi: https://doi.org/10.1021/acs.orglett.7b01074.
Nan G, Shi Q, Shuai Z, Li Z (2011) Phys. Chem. Chem. Phys. 13: 9736—9746. Doi: https://doi.org/10.1039/C1CP00001B.
Ośmiałowski B, Raczyńska ED, Krygowski TM (2006) J Org Chem 71(10): 3727—3736. Doi: https://doi.org/10.1021/jo052615q.
Runge E, Gross EKU (1984) Phys. Rev. Lett. 52: 997—1000. doi: https://doi.org/10.1103/PhysRevLett.52.997.
Sakamoto Y, Suzuki T (2013) J. Am. Chem. Soc. 135(38): 14074—14077. Doi: https://doi.org/10.1021/ja407842z.
Sakanoue K, Motoda M, Sugimoto M, Sakaki S (1999) J Phys Chem A 103: 5551—5556. Doi: https://doi.org/10.1021/jp990206q.
Scholl R; Meyer K (1932) Ber. Dtsch. Chem. Ges. 65: 902. Doi: https://doi.org/10.1002/cber.19370701104.
Sigma Aldrich (2019) website: https://www.sigmaaldrich.com/.
Simon S, Duran M, Dannenberg JJ (1996) J. Chem. Phys. 105: 11024—11031. Doi: https://doi.org/10.1063/1.472902.
Wang L, Li P, Xu B, Zhang H, Tian W (2014) Org. Electron. 15: 2476—2485. Doi: https://doi.org/10.1016/j.orgel.2014.07.003.
Xantheas SS (1996) J. Chem. Phys. 104: 8821—8824. Doi: https://doi.org/10.1063/1.471605.
Xiong X, Deng CL, Li Z, Peng XS, Wong HNC (2017) Org. Chem. Front. 4(5): 682—687. Doi: https://doi.org/10.1039/C6QO00662K.
Yakuphanoglu F, Mansouri S, Bourguiga R (2012) Synt. Met. 162: 918—923. Doi: https://doi.org/10.1016/j.synthmet.2012.04.003.
Yamamoto K, Harada T, Nakazaki M, Naka T, Kai Y, Harada S, Kasai N (1983) J. Am. Chem. Soc. 105: 7171. Doi: https://doi.org/10.1021/ja00362a025.
Zheng J, Xu X, Truhlar DG (2011) Theor Chem Acc 128: 295. Doi: https://doi.org/10.1007/s00214-010-0846-z.